

Geometric and level set tomography using ensemble Kalman inversion

Jack B. Muir¹ and Victor C. Tsai²

¹*Seismological Laboratory, Division of Geological and Planetary Sciences, California Institute of Technology, Pasadena, CA 91125, USA. E-mail: jmuir@gps.caltech.edu*

²*Department of Earth, Environmental and Planetary Sciences, Brown University, Providence, RI 02912, USA*

Accepted 2019 October 17. Received 2019 October 13; in original form 2019 June 11

SUMMARY

Tomography is one of the cornerstones of geophysics, enabling detailed spatial descriptions of otherwise invisible processes. However, due to the fundamental ill-posedness of tomography problems, the choice of parametrizations and regularizations for inversion significantly affect the result. Parametrizations for geophysical tomography typically reflect the mathematical structure of the inverse problem. We propose, instead, to parametrize the tomographic inverse problem using a geologically motivated approach. We build a model from explicit geological units that reflect the *a priori* knowledge of the problem. To solve the resulting large-scale non-linear inverse problem, we employ the efficient Ensemble Kalman Inversion scheme, a highly parallelizable, iteratively regularizing optimizer that uses the ensemble Kalman filter to perform a derivative-free approximation of the general iteratively regularized Levenberg–Marquardt method. The combination of a model specification framework that explicitly encodes geological structure and a robust, derivative-free optimizer enables the solution of complex inverse problems involving non-differentiable forward solvers and significant *a priori* knowledge. We illustrate the model specification framework using synthetic and real data examples of near-surface seismic tomography using the factored eikonal fast marching method as a forward solver for first arrival traveltimes. The geometrical and level set framework allows us to describe geophysical hypotheses in concrete terms, and then optimize and test these hypotheses, helping us to answer targeted geophysical questions.

Key words: Inverse theory; Tomography; Crustal imaging.

1 INTRODUCTION

Geophysical imaging methods, in particular seismic imaging, have offered the strongest constraints on the geometry and material parameters of the internal features of the Earth. Since the origin of geophysical inverse theory in the 1970s (e.g. Backus & Gilbert 1968; Aki *et al.* 1977; Dziewonski *et al.* 1977), imaging methods have rapidly progressed with increasing computational resources, from small-scale linear tomography models to regional and global scale inversions fully utilizing the physics of the governing forward model (e.g. Rawlinson *et al.* 2010). Despite these significant advancements, the interpretability of even well-constrained high-resolution seismic imaging results has remained challenging at regional and global scales, resulting in significant disagreements for the implications of seismic images (e.g. Foulger *et al.* 2013). The potentially most significant underlying reason is the ill-posed nature of the inverse problem. Since the Earth is a 3-D continuous body, and our data are finitely distributed on or near the surface, there can never be a unique solution to the full continuum inverse prob-

lem. This ill-posedness necessitates regularization in imaging, either through explicit Tikhonov type additions to the data misfit function, which are equivalent in the Bayesian formulation to assumptions about the prior distribution of model parameters, or through implicit regularization via basis truncation (Parker 1994; Tarantola 2005; Rawlinson *et al.* 2014). Alternatively, some researchers have sought to use intuition informed by geodynamical considerations to create *ad hoc* images of the Earth through waveform modelling (Ni *et al.* 2002; Song *et al.* 2009; Sun *et al.* 2016; Ko *et al.* 2017). These waveform modelling approaches are particularly important at higher frequencies (~ 1 Hz) where a combination of computational expense and required model complexity have precluded formal tomographic solutions at regional and global scales. Both the inverse problem approach and the waveform modelling approach have deficiencies. In the latter case, significant expert knowledge is required, and it is likely that only a limited range of candidate models will be tested. The former case does not rely on direct human intervention and is consequently potentially more objective, but the damping and smoothing regularization almost universally used create undesirable

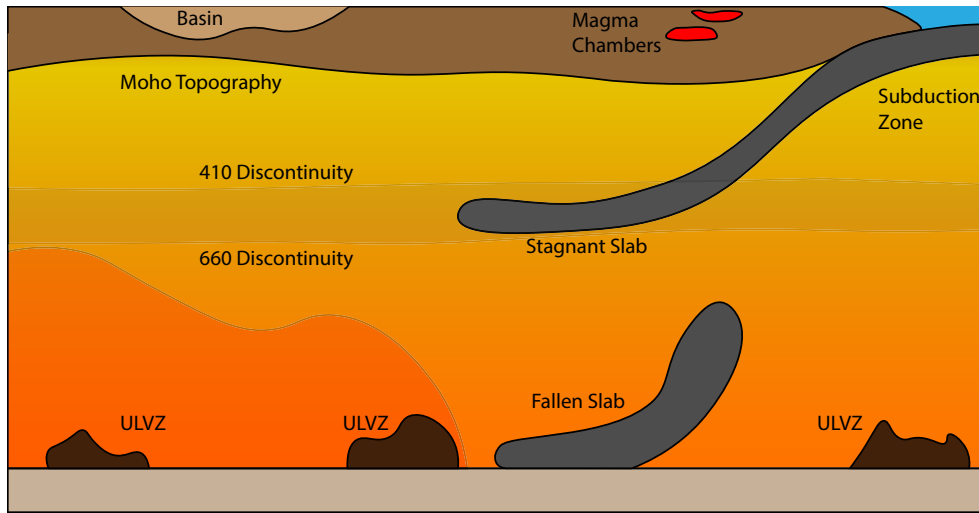


Figure 1. Schematic of the types of imaging targets that represent distinct domains with different geophysical properties; these targets are candidates for our proposed methodology.

tomographic artefacts such as smeared rays and false compensating wave speeds near imaging targets as the misfit function attempts to balance penalties from the data and regularization.

Recent developments in Markov Chain Monte Carlo (MCMC) driven Bayesian tomography have helped to characterize the uncertainty of the results of seismic images (Tarantola 2005), including the degree of data noise and model complexity in the now popular hierarchical transdimensional formulation (Bodin & Sambridge 2009). These uncertainty measures can help one to understand poorly constrained parts of the resulting images, allowing more confidence in the predictions drawn from them. Recent results in transdimensional Bayesian tomography have highlighted the important impact of assumptions about the parametrization of internal boundaries on inversion results (Roy & Romanowicz 2017; Gao & Lekić 2018). Unlike the waveform modelling approach, which relies on strong *a priori* expectations about what potential structures may look like, seismic tomography in both deterministic and MCMC driven forms has typically only loosely prescribed the forms of acceptable models. We assert that in many cases, strong *a priori* knowledge does in fact exist, and that utilizing it can potentially significantly improve the resulting image in the inverse problem context. In addition, where intuition permits a range of potentially feasible geological structures, explicitly modelling these options enables us to evaluate them within a hypothesis testing framework, quantitatively ranking potential models and rejecting models that do not fit the data (Claeskens 2016).

At local scales, objectives of interest include the imaging of anomalous bodies such as tunnels or salt packages, geometric distortions such as faults, and stratigraphic interfaces. At the regional and global scale, there are clear targets of opportunity for which we have strong information from high-frequency waveforms that sharp physical contrasts exist, such as perturbations in important radial discontinuities (the Moho, 410 and 660 discontinuities) and abrupt localized features (slabs, ultra-low velocity zones [ULVZs], sedimentary basins). Specialized methods, such as receiver function analysis, exist to image these structures but they are difficult to use in a traditional tomographic framework. Parametrizing the tomographic inverse problem in such a way that these boundaries are explicitly modelled may help to overcome this limitation. This

observation leads to the fundamental idea of this study, which is to pose the geophysical inverse problem as an optimization of explicitly defined geologic structures. Candidate structures for our proposed methodology are shown in Fig. 1. Defining the inverse problem in this way allows us to better test hypotheses formulated using our *a priori* knowledge, as these hypotheses can be directly modelled. Viewed from another perspective, our inverse framework places waveform-modelling type approaches on a more rigorous footing by allowing greater flexibility in the range of permitted models and supplying the tools necessary for handling larger scale inversions than is possible using an exhaustive full model-space search. An alternative to our explicit modelling viewpoint would be use of the null-space shuttle, which allows *a priori* information to be added after an optimal solution is obtained (Deal & Nolet 1996; de Wit *et al.* 2012; Fichtner & Zunino 2019).

The purpose of this paper is threefold. The first part will describe a method of defining Earth models that allows for flexible modelling of explicit structures, enabling an improvement in the interpretability of inverse problems. Second, we will introduce from the inverse problem literature a derivative-free optimizer based on the Ensemble Kalman Filter, known as Ensemble Kalman Inversion (EKI), and further describe the details of the algorithm for a geoscience audience. Finally, we will illustrate the use of our model definition scheme and EKI to solve nonlinear traveltimes tomography problems.

2 MODEL SPECIFICATION

Parametrization is a fundamental design choice present in all geophysical inverse problems. Parametrizations must seek to accurately represent potential Earth structure, interface with forward solvers, closely predict the data, and lead to solutions of the inverse problem that can be stabilized against the effect of data noise. These potentially conflicting goals have led to a profusion of different parametrization schemes, ranging from simple Cartesian block models, to more exotic basis function sets or spectral domain methods, to irregular multiscale parametrizations designed to tune model complexity to match the data (Rawlinson *et al.* 2010). In this study, we aim to introduce a parametrization designed to intuitively

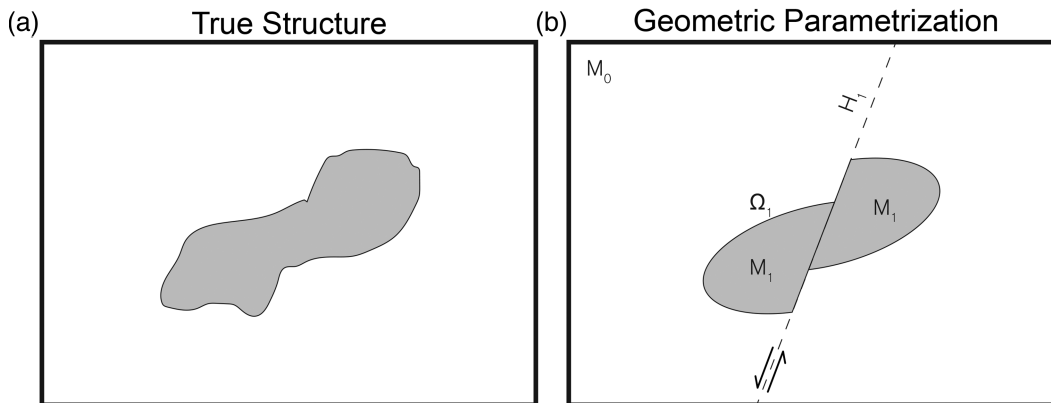


Figure 2. Schematic of the geologically motivated parametrization proposed by this study. (a) Schematic of a body in the Earth that is the imaging target, for which we have some *a priori* knowledge. (b) Schematic of a potential geometric parametrization of the body which we optimize using EKI. M_0 encodes the background model, while Ω_1 and M_1 are the boundary and interior properties of the first model layer, respectively. H_1 is a deformation rule that further alters the model.

describe geological features. Because the model is built up from discrete units that are fixed *a priori*, we use the term model specification rather than parametrization; this highlights that the researcher explicitly introduces their *a priori* knowledge into the inverse problem by determining the number and type of geological features solved for, and also emphasizes that the model is independent of the form of discretization used to solve the forward problem.

In the inverse problem context, a model specification for domain X must provide a set of P functions $\{F_p(x)\}_{p=1}^P$ that determine the P material properties of interest at an arbitrary point $x \in X$. Our model specification framework describes the inversion domain X via a set of simple layers. The base layer defines a background, or reference, model M_0 . The background model has a set of material property functions $F_p(x; M_0)$ that are defined for $x \in X$. So defined, the background model could range from a homogeneous space to a fully 3-D model depending on *a priori* knowledge. On top of the base layer, J objects M_j are defined, each with their own geometries $\Omega_j \subseteq X$ and material parameter functions $F_p(x; M_j)$. We define F_p for a collection of objects as $F_p(x; \{M_j\}_{j=0}^J) = F_p(x; M_{j'})$ where j' is the largest integer with $x \in \Omega_{j'}$ —in concrete terms, we select the topmost layer that contains x , reverting to the background if no higher layers are available. Once the objects are assembled, K deformations (such as faults) are included. The deformations are defined by invertible functions $H_k(x), X \rightarrow X$. To evaluate the model at a particular point in space, these deformations are reversed, so that $F_p(x; \{M_j\}_{j=0}^J, \{H_k\}_{k=1}^K) = F_p(x'; \{M_j\}_{j=0}^J)$ where $x' = H_1^{-1} \circ H_2^{-1} \circ \dots \circ H_K^{-1}(x)$. These operations are shown schematically in Fig. 2. Fig. 2(a) shows an imaging target, while Fig. 2(b) shows a geometric parametrization for the body that can be specified using our parametrization framework, and optimized using EKI to fit available geophysical data.

In the applications discussed in this paper, we are typically interested in describing the interface between two or more geologic units (i.e. the boundaries of regions Ω_j). If the interface is expected to be relatively simple—for instance, if we were attempting to image a near-surface tunnel—then an explicit description of the interface is convenient. An explicit description may be based on deformed geometric primitives, or by describing the locations of spline knots or polygon vertices etc. These explicit definitions have the advantage of reducing the number of parameters required to describe interfaces. However, they are relatively inflexible descriptions, especially when data requires that the topology of the interface should be different from that assumed by the explicit definition (for instance, if two

bodies should be merged into one or vice versa). These situations may require the use of transdimensional methods in which model parameters are added and removed, which significantly increases the complexity of the inverse problem.

Alternatively, object boundaries may be defined implicitly by means of an auxiliary function. Implicit definitions handle complex boundaries and changes in topology, while avoiding the need to change the number of parameters during the inversion. In the following sections, we describe the level set method as a way of implicitly defining object boundaries, and Gaussian random fields as a means of controlling the behaviour of level set functions.

2.1 The level set method

The level set method partitions space into disjoint regions by considering contour lines of a set of n continuous auxiliary functions $\{\phi_i\}_{i=1}^n$. The rationale behind the method is that discontinuous fields can be represented in this way by continuous fields of a higher dimension, which often makes the handling of boundaries more mathematically tractable. Associated with the auxiliary fields are regional parameter fields $\{A_j\}_{j=1}^N$ that describe the value of the parameter of interest within a region. To construct a parameter field F described by level sets, we may use either a combinatoric or a procedural definition. In this work, we employ the procedural definition as it is simpler to implement and combine with other elements of our model definition; however, it does not allow for explicit differentiation of the model. The more commonly used combinatoric definition is given in the appendix for comparison.

Procedural Definition: For N regional parameter fields of interest, set n such that $N = n$. Then $F(x) = A_i(x)$ for the largest i such that $\phi_i(x) > 0$. In this procedural definition, where multiple ϕ are non-zero, we ‘paint over’ with increasing i in a similar fashion to other elements of our model definition framework. Each auxiliary field is individually associated with a spatial region and its associated parameter field, which aids intuition.

Implicit definition of potentially discontinuous boundaries via the level set method has been actively developed since its introduction for the solution of interface evolution problems (Osher & Sethian 1988). In the level set method, an interface is represented by a particular contour on a continuous auxiliary field, examples of which are shown in Fig. 3. Level-set based tomographic methods have recently been intensively studied in the context of Electrical

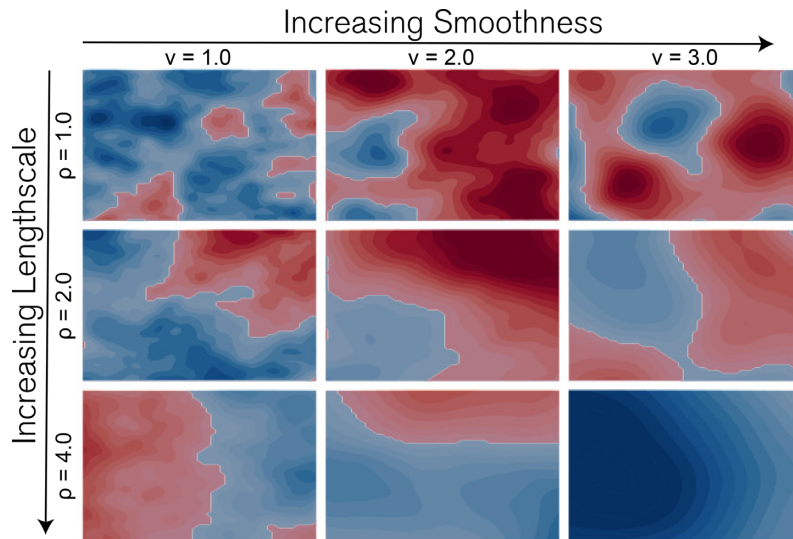


Figure 3. A table of sample zero-mean Gaussian random fields (GRFs) shown by continuous contours. These are overlain by a transparent two-colour image showing a possible level set partition into two fields, defined by the zero contour level of the GRFs. The underlying continuous GRFs, which are visible underneath the two-colour image, give rise to the discontinuous final level set partitioning.

Impedance Tomography (EIT, also known as resistivity tomography, e.g. Chung *et al.* 2005), hydrology (Cardiff & Kitanidis 2009; Iglesias *et al.* 2013), and in various exploration geophysics contexts, especially crosswell seismic tomography and to a more limited extent gravity and magnetic applications (Isakov *et al.* 2011; Zheglova *et al.* 2013; Li *et al.* 2014; Lu & Qian 2015; Li & Qian 2016; Li *et al.* 2017; Zheglova *et al.* 2018). Existing work has typically assumed piecewise constant fields, often of prescribed value, as this strong *a priori* knowledge is often available in exploration contexts. Under this framework, authors have found significantly improved reconstruction of interfaces compared to the smoothed images available from traditional Tikhonov regularized tomographic methods. Work within the geophysics community has exclusively employed the level-set evolution equation, which requires the calculation of the Fréchet derivative of the data misfit functional with respect to the level set function. The misfit functional is typically equipped with regularization that penalizes longer interface lengths (i.e. Total Variation, or TV regularization; Osher *et al.* 2005). The level-set evolution equation allows for efficient inversion but restricts the applicability of the level set formulation to contexts for which the Fréchet derivatives are available. Additionally, existing applications using the level set evolution equation (Li *et al.* 2017; Zheglova *et al.* 2018) require significantly more mathematical machinery when multiple level sets are used, limiting their applicability to complex models. When the derivatives are not available, for example when using externally supplied black-box forward models, the level-set evolution equation and also traditional iterative gradient-based tomographic methods break down. An alternative to TV regularization of level sets is specification of a Gaussian random field prior for the auxiliary field used to generate the level set (e.g. Chada *et al.* 2018). Using a Gaussian random field prior allows explicit control of the dominant length scale and roughness of the resultant level set, as shown in Fig. 3. A possible alternative would be to learn appropriate basis function representations of the level-set auxiliary field from data using a dictionary learning approach (e.g. Bianco & Gerstoft 2018). Due to its conceptual simplicity, the Gaussian random field based level-set approach is taken in the examples below to specify the boundary of object layers with our model specification framework.

2.2 Gaussian random fields

Gaussian random fields (GRFs, also commonly referred to as Gaussian processes, especially in 1-D applications) have a long history in geostatistics where they provide the framework for kriging estimators of fields with observed training data (Chiles & Delfiner 2012). In the inverse problem setting, the quantities of interest are not observed directly. For the linear or weakly nonlinear case, Hansen *et al.* (2006) has supplied theory for conditioning GRF priors on averaged observations such as traveltimes in fixed ray path tomography. An intriguing further development in applying GRFs to geophysical inverse problems has recently been provided by Ray & Myer (2019), which utilizes transdimensional MCMC for sampling training points on which the GRFs are conditioned. In this study, we use GRF priors, without conditioning on training data points, for the auxiliary fields used by the level set method. Thus, the material parameter fields are not determined by the GRFs directly, but rather by a nonlinear transform of them that can encode abrupt changes in material properties.

A comprehensive review of GRFs is given by Rasmussen & Williams (2006); here we offer a brief summary of definitions that are important to the model specification scheme outlined in this study. A scalar valued GRF on \mathbb{R}^n is a spatial process analogous to a Gaussian distribution. It is defined by a mean function $m(x)$ and symmetric covariance function $C(x, y) = C(y, x)$ and has the property that any finite set of points $\{x_k\}_{k=1}^M$ on the field are distributed as a multivariate Gaussian distribution $N(\mathbf{m}, \Sigma)$ with

$$\mathbf{m} = \begin{bmatrix} m(x_1) \\ \vdots \\ m(x_M) \end{bmatrix}, \quad \Sigma = \begin{bmatrix} C(x_1, x_1) & \dots & C(x_1, x_M) \\ \vdots & \ddots & \vdots \\ C(x_M, x_1) & \dots & C(x_M, x_M) \end{bmatrix}. \quad (1)$$

The covariance function encodes the GRF's spatial correlation behaviour, and may be anisotropic and spatially varying (non-stationary); in many typical applications, a subclass of isotropic, stationary GRFs are employed for which only the distance between x and y matters, i.e. $C(x, y) = C(\|x - y\|)$. Within this class, the prototypical covariance functions with spatially constant variance

σ^2 are the exponential covariance with characteristic length scale l

$$C(x, y) = \sigma^2 \exp\left(-\frac{\|x - y\|}{l}\right), \quad (2)$$

and the Matérn covariance function with smoothness parameter ν and length scale parameter ρ

$$C(x, y) = \sigma^2 \frac{2^{1-\nu}}{\Gamma(\nu)} \left(\frac{\sqrt{2\nu}\|x - y\|}{\rho}\right)^\nu K_\nu\left(\frac{\sqrt{2\nu}\|x - y\|}{\rho}\right), \quad (3)$$

where Γ is the gamma function and K_ν is the modified Bessel function of the second kind. The Matérn covariance function includes the exponential covariance function (as well as the squared-exponential variance function) as a special case. Fig. 3 shows a table of example GRFs defined by Matérn covariances of different length scales and smoothness parameters, as well as level set partitions that can be defined by them. GRFs form a useful class of fields for defining boundaries in models using the level set method as they encode a wide range of potential prior information that can be tailored to a particular geophysical problem.

3 ENSEMBLE KALMAN INVERSION

The model specification framework proposed in this paper aims to map the *a priori* information of a researcher into an Earth model in a way that is independent of the computational requirements of the forward solver used by the inverse problem. While defining models in this fashion is advantageous from the perspectives of ease of usage and interpretation, it potentially makes derivatives of the desired geophysical observables with respect to model parameters difficult to calculate using fast analytic or adjoint methods—that is, the model function F may not be easily differentiable. Additionally, derivatives of the physical model may not be available when using closed source or legacy code. Since explicit calculation of derivatives via finite differencing is intractable for models with many parameters, and we wish to maintain solver independence, in general precluding the use of algorithmic automatic differentiation, we are motivated to employ an efficient derivative-free optimizer for inverse problems defined using our model specification framework. In particular, we have employed the Ensemble Kalman Inversion optimizer (Iglesias *et al.* 2013), which we define below.

The Ensemble Kalman Inversion (EKI) scheme was introduced by Iglesias *et al.* (2013) as a derivative-free ensemble-based approximation of the iteratively regularized Levenberg–Marquardt (LM) inversion scheme (Hanke 1997). Further development has resulted in applications to hydraulic reservoir modelling (Iglesias 2015; Chada *et al.* 2018), electrical impedance tomography (Chada *et al.* 2018), and for optimizing neural-network parameters in machine learning (Kovachki & Stuart 2019). For comparison, we first describe the regularizing LM scheme from which the EKI scheme is derived. We closely follow the development in Iglesias (2016).

Iteratively Regularized Levenberg–Marquardt scheme: The iteratively regularized LM scheme considers an inverse problem with model parameters $u \in X$ and data $y \in Y$. X and Y are Hilbert spaces with appropriate norms $\|\cdot\|_X$ and $\|\cdot\|_Y$; in a geoscience application X will typically be either a finite dimensional space \mathbb{R}^P or a function space on \mathbb{R}^P and Y will be a finite dimensional observation space \mathbb{R}^M . We assume that $y = G(u^\dagger) + \eta$ for some model operator G , ‘true’ set of model parameters u^\dagger , and noise η . Using our model framework, we typically have a set of model parameters that are transformed by the model function F to the physical model of interest on an evaluation grid, which are then input into a forward

solver H so that $G(u) = H(F(u))$. We assume *a priori* knowledge of the noise level

$$\eta = \|\Gamma^{-1/2}(y - G(u^\dagger))\|_Y, \quad (4)$$

where Γ is an operator that encodes the measurement precision, so that the absolute misfit $(y - G(u))$ is weighted to account for the quality of measurements. For finite dimensional observations equipped with the normal Euclidean norm, if we assume that $\eta \sim N(0, \sigma)$ (i.e. Gaussian noise with variance σ^2) and we set $\Gamma = I$ so that observations are equally weighted, then $\eta \approx \sigma\sqrt{M}$ where M is equal to the number of observations.

The objective of any iteratively regularized scheme is to find a model u^n that is a stable approximation of u^\dagger with respect to the noise in the sense that as $\eta \rightarrow 0$, then $u^n \rightarrow u^*$ for some $u^* \in X$ with $G(u^*) = G(u^\dagger)$. In contrast to standard Tikhonov regularization methods, in which the problem is explicitly regularized and then optimized, iteratively regularized schemes fundamentally seek an approximate solution to the unregularized problem but stabilize the parameter updates and terminate at an appropriate level of fitting to avoid being dominated by noise. In the LM scheme, this condition is achieved by solving a succession of Tikhonov regularized updates with regularizing parameter α_n

$$u_{n+1} = u + v^*, \quad (5)$$

$$v^* = \arg \min_{v \in X} (\|\Gamma^{-1/2}(y - G(u_n) - DG(u_n)v)\|_Y^2 + \alpha_n \|C^{-1/2}v\|_X^2), \quad (6)$$

where $DG(u_n)$ is the Fréchet derivative of G in respect to u , so that $y - G(u_n) - DG(u_n)v$ is a linear approximation of the misfit about u_n . C is an operator $X \rightarrow X$ that encodes regularity or prior information on X , and α_n controls the strength of the regularization at each update step. Note that within the LM scheme, the linear term of the first quadratic form gives rise to a steepest descent update, while the second order term gives the Gauss–Newton approximation of the Hessian (see Appendix A2 for the derivation in finite dimensions). The desired stable convergence property of LM was shown by Hanke (1997) to require that α_n at each iteration must satisfy

$$\rho \|\Gamma^{-1/2}(y - G(u_n))\|_Y \leq \alpha_n \|\Gamma^{-1/2}(y - G(u_n) - DG(u_n)v^*)\|_Y \quad (7)$$

for a tuning parameter $\rho \in (0, 1)$ that is set *a priori* and fixed for all iterations. The scheme is terminated when

$$\|\Gamma^{-1/2}(y - G(u_n))\|_Y \leq \tau \eta < \|\Gamma^{-1/2}(y - G(u_{n-1}))\|_Y \quad (8)$$

for some fixed $\tau > 1/\rho$, where this inequality is required to ensure stable convergence of the scheme (Hanke 1997). This termination criterion is a form of Morozov’s discrepancy principle (Scherzer 1993), and ensures that the LM scheme does not overfit to the noise; without the termination criterion the scheme is equivalent to a modification of a standard unregularized Levenberg–Marquardt optimizer. Eq. (6) can be shown to be equivalent to the explicit update

$$u_{n+1} = u_n + (DG^*(u_n)\Gamma^{-1}DG(u_n) + \alpha_n C^{-1})^{-1} \times DG^*(u_n)\Gamma^{-1}(y - G(u_n)), \quad (9)$$

with DG^* the adjoint operator of DG (Iglesias & Dawson 2013). For finite dimensional X , the m th component of DG is $D_m G(u_n) = J(u_n) \cdot e_m$ where J is the Jacobian of G and e_m is the unit vector for m ; eq. (9) then simplifies to the standard finite dimensional LM update

$$u_{n+1} = u_n + (J(u_n)^T \Gamma^{-1} J(u_n) + \alpha C^{-1})^{-1} J(u_n)^T \Gamma^{-1} (y - G(u_n)). \quad (10)$$

When the Fréchet derivative of G is available, the iteratively regularizing LM scheme provides a useful framework for the general solution of nonlinear inverse problems, and has been applied successfully in geophysical applications for groundwater flow (Hanke 1997; Iglesias & Dawson 2013).

Ensemble Kalman Inversion scheme: The Ensemble Kalman Inversion (EKI) scheme is an ensemble approximation of the iteratively regularized LM scheme. The general concept is to update an ensemble of particles (where each particle represents a realization of the model) using the ensemble Kalman filter (Evensen 1994; Iglesias 2016). Ensemble Kalman filters have received recent attention in the seismology community as a means of uncertainty quantification in large-scale full-waveform inverse problems (Thurin *et al.* 2017; Eikrem *et al.* 2019), although this usage is still in its preliminary stages. In this study, we utilize the EKI dynamic purely as a high-performance iteratively regularized optimizer.

The dynamics driving the EKI ensemble are designed to drive the mean of the particles towards the solution of the inverse problem of interest (Iglesias *et al.* 2013). At each step, the ensemble of particles solves an approximate Tikhonov regularized update with iteration-dependent regularization α_n , the strength of which is controlled by a global regularization parameter ρ (Iglesias 2015). We let the ensemble at iteration n be $\{u_n^{(j)}\}_{j=1}^J$ where J is the number of ensemble members. Means of collections are denoted by overbars (i.e. \bar{u}_n is the mean over the collection of $\{u_n^{(j)}\}_{j=1}^J$). Approximating $G(u_n^{(j)})$ to first order about the mean of the ensemble

$$G(u_n^{(j)}) \approx G(\bar{u}_n) + DG(\bar{u}_n)(u_n^{(j)} - \bar{u}_n). \quad (11)$$

Iglesias (2016) shows that using this approximation, explicit calculation of the Fréchet derivative $DG(u)$ may be eliminated, leading to an approximation of the iteratively regularized LM scheme by the following algorithm:

Initialization Draw $\{u_n^{(j)}\}_{j=1}^J$ ensemble members from prior distribution. Set $\rho \in (0, 1)$ and $\tau > 1/\rho$. Then for $n = 0, 1, \dots$

Prediction Evaluate $w_n^{(j)} = G(u_n^{(j)})$; calculate \bar{w}_n

Termination If $\|\Gamma^{-1/2}(y - \bar{w}_n)\| \leq \tau\eta$, terminate and output \bar{u}_n as the solution

Analysis At each iteration, an ensemble of perturbed data $\{y_n^{(j)}\}_{j=1}^J$ is generated with additional noise $y_n^{(j)} = y + \eta$. Addition of extra noise helps the ensemble to better explore parameter space by preventing the ensemble from converging to a single point from which ensemble gradients cannot be computed. Let $\langle \cdot, \cdot \rangle_Y$ being the inner product on Y and define covariance operators C_n^{uw} and C_n^{ww} by

$$C_n^{ww}(\cdot) = \frac{1}{J-1} \sum_{j=1}^J (G(u_n^{(j)}) - \bar{w}_n)(G(u_n^{(j)}) - \bar{w}_n, \cdot)_Y, \quad (12)$$

$$C_n^{uw}(\cdot) = \frac{1}{J-1} \sum_{j=1}^J (u_n^{(j)} - \bar{u}_n)(G(u_n^{(j)}) - \bar{w}_n, \cdot)_Y, \quad (13)$$

then update the model ensemble $\{u_n^{(j)}\}$ with the ensemble of perturbed data $\{y_n^{(j)}\}_{j=1}^J$ by

$$u_{n+1}^{(j)} = u_n^{(j)} + C_n^{uw}(C_n^{ww} + \alpha_n \Gamma)^{-1}(y_n^{(j)} - w_n^{(j)}), \quad (14)$$

where α_n is heuristically chosen to be $\alpha_n = 2^i \alpha_0$, with α_0 an initial guess, such that $i \geq 0$ is the first integer with

$$\alpha_n \|\Gamma^{1/2}(C_n^{ww} + \alpha_n \Gamma)^{-1}(y - \bar{w}_n)\| \geq \rho \|\Gamma^{-1/2}(y - \bar{w}_n)\|. \quad (15)$$

α_0 , ρ and τ are tuning parameters of the scheme; typically $\alpha_0 = 2$ so that $\alpha_n \geq 1$ —the choice of $\alpha_n = 2^i \alpha_0$ is a heuristic that tries to balance choosing as small as possible α_n without computing

eq. (15) many times for each analysis step; theoretically any α_n that satisfies eq. (15) is acceptable, but this heuristic provides a good balance of computational effort without overregularizing. Higher values of ρ provide greater regularization by forcing larger α_n ; this typically also results in more iterations until the termination criterion is reached (Iglesias 2016). If P is the dimension of the model space (potentially after discretization in the case where G operates on fields) and M is the number of observations, then C_n^{uw} is a $P \times M$ matrix and C_n^{ww} is an $M \times M$ matrix. For large data and model spaces, constructing and especially inverting these matrices can be very expensive— $O(M^3)$ for the construction of $(C_n^{ww} + \alpha_n \Gamma)^{-1}$. However, due to their construction, both covariance matrices are of rank at most $\min(J-1, M)$. Consequently, for $J \ll M$, it is more efficient to implement them within the algorithm as operators defined by eqs (12) and (13). For constructing the inverse, we employ a low rank approximation of C_n^{ww} to compute the approximate Hermitian eigen decomposition of the operator, as it is symmetric positive semi-definite by construction (Halko *et al.* 2011). The low rank approximation is exact if an approximation of rank $J-1$ is sought. This decomposition allows us to write

$$C_n^{ww} = Q \Lambda Q^T, \quad (16)$$

where Λ is a square diagonal matrix of dimension at most $(J-1) \times (J-1)$ containing the largest eigenvalues of C_n^{ww} and Q , which is a M by at most $J-1$ matrix, has columns equal to the eigenvectors of C_n^{ww} corresponding to the elements of Λ . We may then use the Woodbury matrix identity to compute

$$\begin{aligned} (C_n^{ww} + \alpha_n \Gamma)^{-1} &= (Q \Lambda Q^T + \alpha_n \Gamma)^{-1} \\ &= \frac{\Gamma^{-1}}{\alpha_n} - \frac{\Gamma^{-1}}{\alpha_n} Q (\Lambda^{-1} + Q^T \Lambda^{-1} Q)^{-1} Q^T \frac{\Gamma^{-1}}{\alpha_n}. \end{aligned} \quad (17)$$

The matrix $(\Lambda^{-1} + Q^T \Lambda^{-1} Q)$ is of dimension at most $(J-1) \times (J-1)$, and all other inverses are of diagonal matrices. Constructing the Hermitian eigendecomposition requires only matrix-vector products (Halko *et al.* 2011); due to the structure of the covariance matrix C_n^{ww} , only J vector-vector products are actually required if we use C_n^{ww} in its operator form. This means that C_n^{ww} never needs to be explicitly constructed, which can result in significant memory savings for large data sets. The cost of constructing the eigendecomposition is amortized across the need to update J ensemble members. Consequently, using a low rank approximation and applying the Woodbury matrix identity can dramatically reduce the cost of updating the ensemble in both number of operations and memory. Fig. 4 shows a schematic of the EKI algorithm applied to a two parameter linear inverse problem. Far from the optimum, ensemble members take scaled gradient descent steps as the regularization provided by $\alpha_n \Gamma$ dominates the dynamics. Closer to the optima, the ensemble becomes more aware of the curvature of the objective as the C_n^{ww} term dominates.

In the basic EKI algorithm, the final model u^0 lies in the span of the initial ensemble. Appropriate choice of the initial ensemble therefore acts to encode prior information into the inverse problem. Within our model specification framework, the actual geological model $F(u)$ used to predict data by the forward solver is a nonlinear transform of the model parameter vector u defining the underlying Gaussian random fields and geometric parameters. This allows significant flexibility even when the underlying space of potential models is constrained to lie within a low-dimension subspace of the full space of models. Specifically, though the final parameter vector \bar{u}_n describing the model specification is in the span of the initial

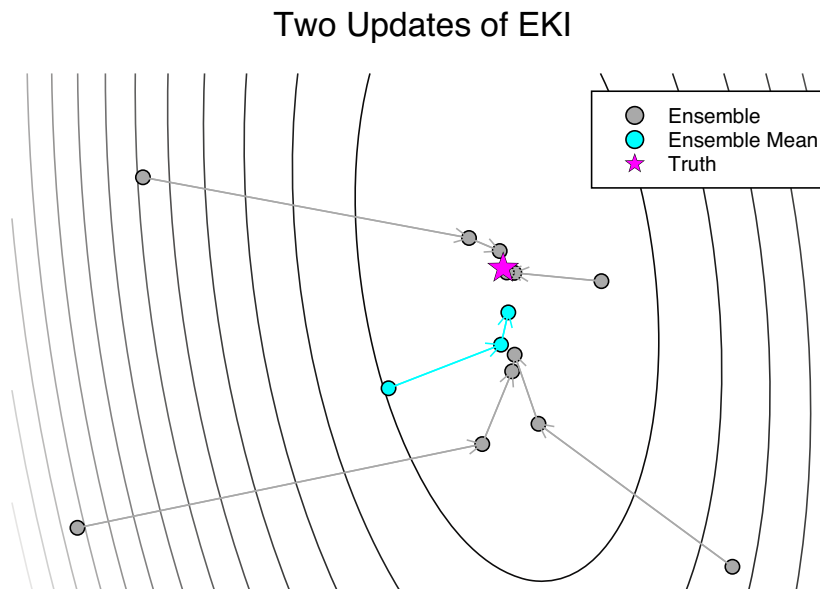


Figure 4. Two updates of the EKI algorithm with four ensemble members for a toy linear objective with two parameters. Elliptical lines show the contours of the objective function.

ensemble $\{u_0^{(j)}\}_{j=1}^J$, the corresponding physical model $F(\bar{u})$ is not necessarily in the span of $\{F(u_0^{(j)})\}_{j=1}^J$.

The EKI algorithm offers several compelling benefits for the derivative-free solution of PDE constrained inverse problems. From a theoretical standpoint, the stable convergence to an approximate solution depending on the noise level is appealing. Furthermore, the scheme is practical, easy to implement, and handles large parameter spaces. In particular, the calculation of the forward models $G(u_n^{(j)})$ and the updates of models $u_{n+1}^{(j)}$ have no interaction between ensemble members. Consequently, these parts of the algorithm are embarrassingly parallelizable and scale trivially to meet available computational resources (Herlihy & Shavit 2011). Since the forward model calculations are typically the most expensive part of the algorithm, this is a particularly useful property. Finally, an important consideration for practical employment of the algorithm is that it allows black-box forward models, such as legacy or proprietary closed-source codes for which derivatives of the misfit function with respect to model parameters are not available, to be used without expensive explicit finite differencing. Compared to obtaining the gradient from the adjoint method, the EKI method uses J forward solves for every step, compared to J_a for an adjoint method, so that the ratio of computational effort is J/J_a if the solution of model updates is negligible in cost. J_a depends on the forward model but is typically 2–3, while the optimum J depends on the problem but is typically larger. Despite this, as the J ensemble members are independent, the ensemble method is particularly amenable to distributed computing even if communication between processes has high latency. Additionally, for non-self-adjoint forward solvers, the EKI algorithm does not utilize a backwards pass and so does not require complex checkpointing schemes for managing storage requirements (e.g. Komatitsch *et al.* 2016), which may be a useful property for some problems.

3.1 Inversion framework summary

The inversion framework presented in this study consists of a geologically motivated parametrization of the Earth, coupled to an

efficient, highly parallelizable and derivative-free solver. Framing geophysical inverse problems as a question of optimizing geological models allows for direct interpretation of the resulting images, and allows practitioners to compare structurally different models against each other. The parametrization scheme described above has the flexibility to describe models ranging from simple 1-D descriptions to fully 3-D, heterogeneous models with structural discontinuities in a consistent format. We have shown that by using the implicit level-set method to define geological domains allows the topology of a model to change to fit the data without changing the parametrization, in contrast to explicit definitions of domains in which the parameters must be added or removed to describe changes in topology, significantly complexifying the inverse problem. Our parametrization framework motivates using a derivative-free optimizer because the resulting models are not necessarily efficiently differentiable, and because a goal of this study is to modularize the inverse problem so that the structure of the model is not tied directly to the forward solver. We employ EKI as the optimizer, as it scales well with computational resources, treats the forward solver as a black box, and incorporates iterative regularization to avoid overfitting the data. Utilizing the inherent low-rank structure of the covariance matrices used by EKI allows even large data sets to be handled efficiently. As an iteratively regularized algorithm, EKI does not include explicit Tikhonov damping and will fit the data to within an assumed noise level, without the biases introduced by these terms. The tuning parameters in the EKI scheme instead control the stability of the convergence and the convergence rate.

4 EXAMPLES

To illustrate the combination of our model parametrization framework and the EKI inversion scheme, we show two synthetic seismic tomography examples and one example using real active source seismic data collected at Carrizo Plains, CA. In all cases, the data are first arrivals of P waves from known source locations, as is typical in an active source seismic experiment. We have chosen this relatively simple forward model to concentrate on the details of the

model specification and the inversion method. We note, however, that both the model specification framework and the EKI solver are independent of the choice of forward model and are not limited to seismic traveltimes tomography; for instance joint inversions incorporating potential methods such as gravity could be used, or full seismic waveforms could be used—noting that for full waveform methods the model specification must be very close to the truth or it is likely that the inverse problem will converge to an unrealistic local minimum.

To calculate the arrival times through the model, we solve the eikonal equation using the fast marching method (Osher & Sethian 1988; Rawlinson & Sambridge 2004). We employ the factored form of the eikonal equation, accounting for the singularity at the source analytically, resulting in significantly improved traveltimes calculations along grid diagonals relative to the basic eikonal method (Treister & Haber 2016). The first example illustrates the advantages of the GRF level-set definition for describing geological domains; the second example shows how our model specification can compose geological objects and deformations; the third example shows that our method is robust for real data and highlights the useful iteratively regularizing properties of the EKI scheme. In the examples that follow, we take GRFs with fixed length scales for simplicity; solving for GRF length scales may be achieved during the inversion by hierarchical EKI (Chada *et al.* 2018).

4.1 Shape recovery in first arrival crosswell tomography

Our first example is an application of the level set method with GRF priors to invert first arrival data in a crosswell geometry using the EKI algorithm—as such, this example uses only a subset of the model description framework described in Section 2. The purpose of this example is to illustrate the advantages of implicitly defining boundaries via the level set method. This type of shape optimization problem may be alternatively solved using the level-set evolution equation (Li *et al.* 2014), however, the GRF based formulation used in this study imposes additional *a priori* constraints on the inverse problem—this example shows that shape recovery is still possible under these constraints. We synthesize data from nine sources in a vertical well with 16 m spacing. We record data in a vertical well 96 m away, with sensors spaced at 4 m, and assume a nominal data picking error of 0.25 ms. We hypothesize a background model of 1000 m s^{-1} velocity, with fast inclusions of 1500 m s^{-1} . The geometry of the true input model is shown in Fig. 5(a).

We assume that we have no knowledge of the number or geometry fast inclusions, while the velocities are known. This makes explicit parametrization of their locations and shapes difficult, as some heuristic must be used to determine the appropriate number and topologies of boundaries. To overcome this issue, we generate an initial ensemble of 200 candidate models using GRF defined level sets, containing a wide range of inclusion topologies—four examples of the starting ensemble are shown in Fig. 5(b), from which we can confirm that the initial ensemble is not strongly tuned to reflect the true input model. The ensemble was generated using a zero-mean Matérn GRF with $\rho = 50 \text{ m}$ and $\nu = 1.5$; the choice of a Matérn GRF with $\nu < 2$ is motivated by a desire to have solutions with somewhat rough boundaries. Therefore, for this example, the parameter vector u consists of the values of the latent field, initially drawn from the Matérn distribution, and the model function F is the level set operator assigning values of the latent field that are greater than 0 to 1500 m s^{-1} , and those below 0 to 1000 m s^{-1} . The forward operator H is the solution of the factored eikonal equation from the

sources to the receivers, and as usual the full forward map may be written as $G(u) = H(F(u))$.

We evolve the initial ensemble using the EKI algorithm using $\rho = 0.75$ and $\tau = 1.6$ until the discrepancy principle termination criterion is satisfied after 40 iterations. The output model and fits to the data are shown in Figs 5(c) and (d). We see that the location and approximate geometries of the three inclusions are recovered, and that the data are well fit by the predicted model.

In this example, regularization is provided by the underlying structure of the GRF used to generate the ensemble. In particular, the wavelength parameter ρ of the Matérn covariance was chosen to be comparable to the size of the inversion domain, which suppresses short wavelength structure. The EKI algorithm, as presented in this paper, produces model parameter outputs in the linear span of the initial ensemble, which has the effect of maintaining the GRF structure throughout the iterations of the inversion. The level set function acts as a nonlinear activation function, allowing the GRF function to produce the shorter length scale features required by the data, even though the GRF length scale is significantly longer. Setting the GRF length scale to be large avoids the introduction of small anomalous features in the final result. Additionally, the discrepancy principle used to terminate EKI serves to avoid overfitting the data; the inversion starts with smooth members of the starting model and evolves greater complexity, stopping immediately once a fit to the data is achieved.

4.2 Determining surface fill depth with a fault

In many geological settings, there may be stronger *a priori* knowledge of potential structures that can be employed in an inversion. A typical example of this would be the inferred presence of faults derived from observed seismicity, surficial rupture or other geological constraints. In this example, we simulate first-break seismic refraction data for a smoothly varying interface between two layers bisected by a vertical fault with some offset—for example, this could be a profile perpendicular to a strike-slip fault with unconsolidated alluvial surface cover. We assume sources spaced every 30 m and receivers spaced every 5 m along a profile 240 m in length. Data were perturbed with 1 ms Gaussian noise to simulate picking error estimated from a real data experiment with equivalent geometry (Example 4.3). The true model is shown in Fig. 6(a). A simple stationary GRF-based level set approach cannot easily represent this kind of model since the smooth covariance structure will suppress the fault, acting similarly to a Tikhonov smoothing regularization. Instead, we explicitly add in the presence of a potential fault in our model description. This has the additional advantage that the parameters related to the fault (e.g. position, dip angle, offset) are immediately physically interpretable. This type of inversion therefore represents a combination of level set inversion and minimum-parameter modelling in the style of Zelt & Smith (1992). The objective of the inverse problem is then to calculate the optimal parameter vector u , which is made up of the GRF latent field describing the interface, the explicit geometrical parametrization of the fault, which consists of the horizontal location of the fault plane, the amount of vertical offset, and the velocities of the two layers. The forward map can again be written $G(u) = H(F(u))$ where F transforms u into the physical model of interest evaluated on a Cartesian solver grid, and H solves the factored eikonal equation. We use EKI with 256 ensemble members to solve the resulting inverse problem, which converged in 28 iterations. Once again, we show four examples of the initial ensemble to illustrate the range of potentially allowable geometries

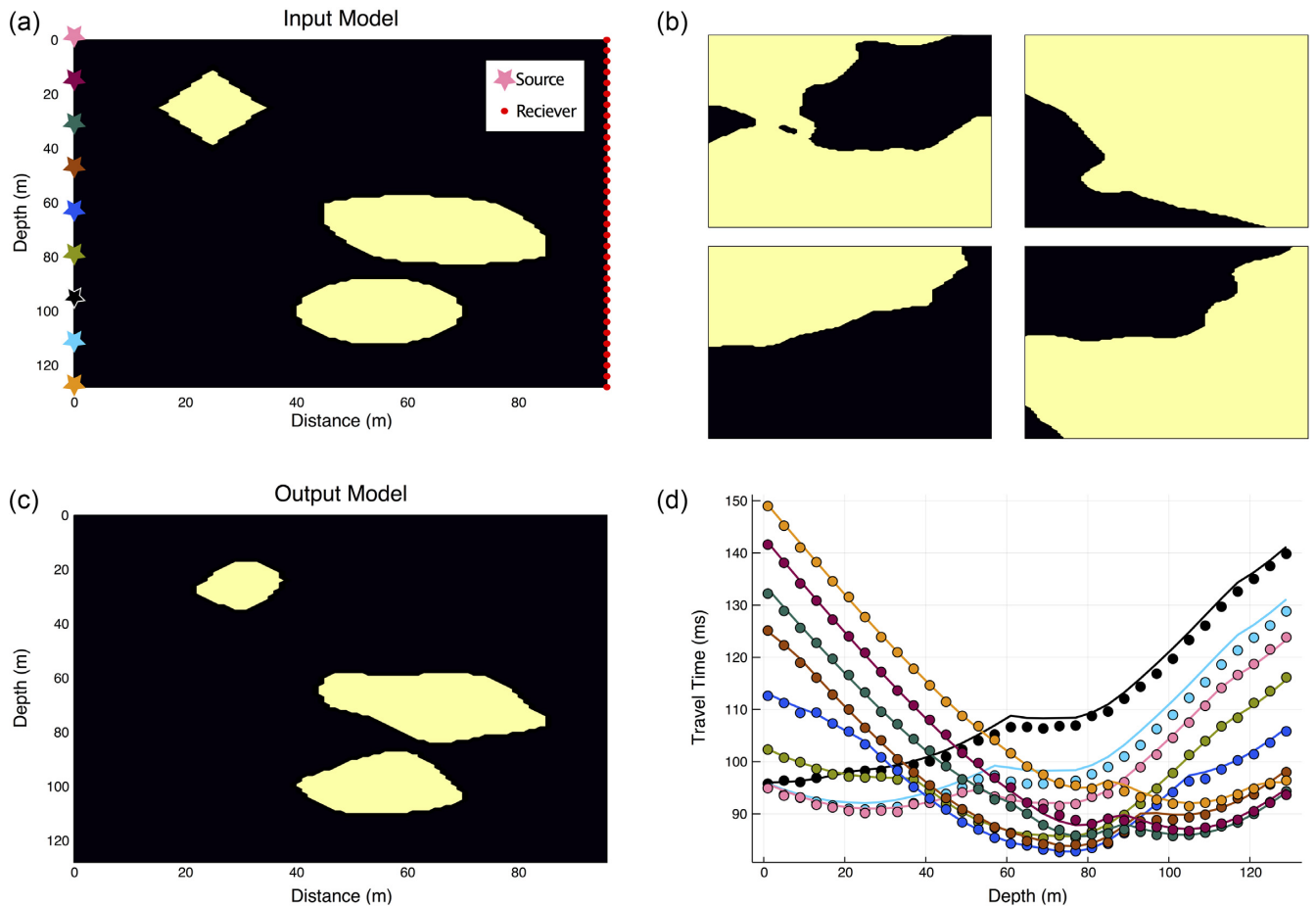


Figure 5. Use of Gaussian random field (GRF) level sets for a crosswell tomography boundary identification problem. (a) The true input model, with source and receiver geometry. The yellow regions are 1500 m s^{-1} , black 1000 m s^{-1} . (b) Four examples of the initial ensemble of models used for EKI. (c) The output model. (d) The data and fit, with colours corresponding to the source colours in (a).

in Fig. 6(b). The final inverted model is shown in Fig. 6(c), together with a comparison in Fig. 6(d) to a traditional ray tracing based tomography performed using the commercial DWTomography Software, which explicitly considers topography and creates a smoothed regularized solution (Geogiga Technology Corporation 2016).

Without a *a priori* knowledge of the expected structures, the traditional refraction tomography smooths the vertical interface and has approximate vertical and horizontal resolution of $\sim 10 \text{ m}$, controlled by the regularization and data quality, as can be seen in Fig. 6(d). Additionally, the L2 regularization used in the traditional tomography promotes a smooth transition from low to high velocity. Assuming we have appropriate knowledge, our level set/geometric parametrization can much better recover the true model. In this case, appropriate knowledge could be prior mapping of a surface rupture of the fault. The question of whether an explicitly layered model such as this is more appropriate than a smooth model requires assessment of the data, as well as any appropriate geologic knowledge at hand.

4.3 Near-surface refraction tomography of the San Andreas Fault at Carrizo Plains

For a final example, we apply our inversion scheme to real seismic refraction data collected on 2017 March 20 at Carrizo Plains, California, USA. Reconstruction of paleoseismicity of the San Andreas Fault (SAF) at Carrizo Plains suggests regular slip of up to

$\sim 5 \text{ m}$ (Ludwig *et al.* 2010; Zielke *et al.* 2010), with trenching implying a potentially $> 10 \text{ m}$ wide band of multiple near-surface fault strands that are likely to be seen as a low velocity damage zone in tomographic images (Akciz *et al.* 2009). Data were collected along a profile of length 240 m, oriented SW to NE, with significant topography, using a 48 channel geophone array. The profile is roughly bisected by the SAF, which can be prominently seen in Fig. 7(a), especially noting the significant stream channel offset near the centre of the image. Remington Industrial 8-gauge charges buried approximately 0.25 m deep generated the active sources at 0, 60, 120, 180 and 235 m along the profile. First arrival times were then handpicked. We consider the data noise to include picking and triggering errors, imprecision in the source and receiver locations, and errors in the recorded surface topography. The true noise distribution is consequently unknown; for this application we will assume data are independent, identically Gaussian distributed with equal variance.

The purpose of this example is primarily to show that the combination of the level set formulation and EKI is practical and stable when applied to real data and to compare it against a traditional tomographic image. Inspection of the data suggests a three layered model. Consequently, we choose to invert for a model vector u that consists of two 1-D GRFs describing layer interfaces and the constant velocities of the three layers. The model function F computes level sets from the GRFs and assigns velocities to the resulting regions in physical space. The explicit topography derived from the

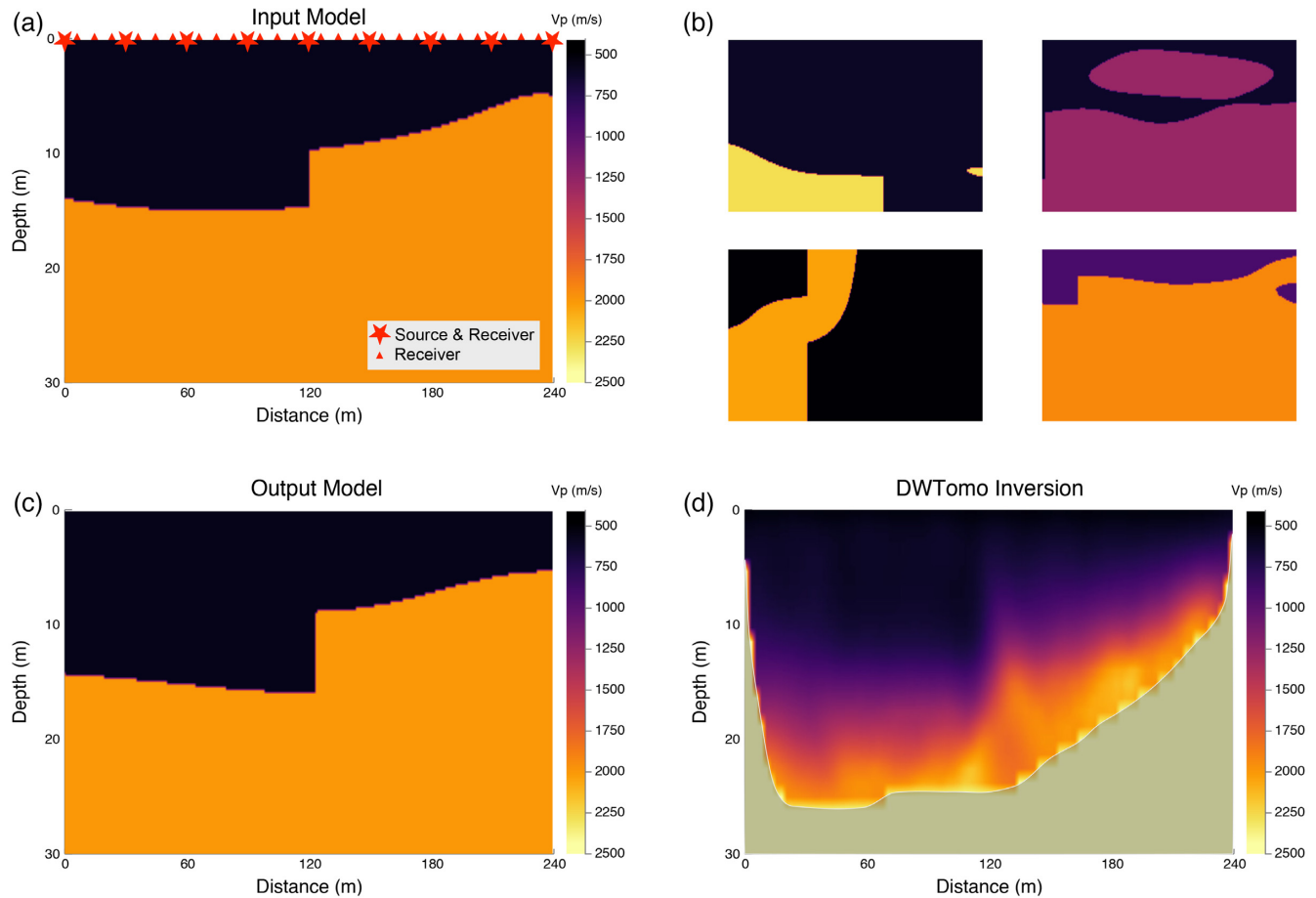


Figure 6. Illustration of using a combination of level sets and explicit geometric parametrizations to recover a subsurface interface offset by a vertical fault. (a) The true input model with source / receiver geometry. (b) Four examples of the initial ensemble of models used for EKI. (c) The output of the inversion. (d) The traditional inversion using DWTomo; the opaque grey mask shows the boundary of the rays calculated by DWTomo.

known locations of the receivers is included in F by linear spline interpolation. In this case, we chose to employ 1-D GRFs to initialize the ensemble for a 2-D model inversion, to avoid overlapping folds in the boundaries between regions. Similarly, in a 3-D setting, 2-D GRFs may be used to introduce a layered structure with no folds. This type of problem could potentially be solved using a multiple-level-set evolution equation method such as that in Li *et al.* (2017), however, as shown in Section A1 the combinatorial complexity of these methods greatly increases with the number of layers, and our GRF formulation provides intrinsic regularity to the solutions which motivates the use of our model specification framework. As previous trenching evidence suggested that the fault was likely to be observed as a distributed damage zone at the length scale of this study, we did not employ any deformation layers in our model description. We chose Matérn GRFs with $\rho = 100$ m, $\nu = 1.5$, and $\sigma = 5$ m. The *a priori* mean depth of the first layer used to generate the EKI ensemble was set to be uniform across the depth range of the model, with the mean depth of the second layer set to be uniformly generated between 0 and 20 m below the first layer. To test the stable convergence properties of EKI, we inverted the data assuming nominal noise standard deviations σ of 6, 4, and 3 ms, with the resulting models shown in Figs 7(d), (f), (h), respectively. Note that we estimated a picking error of approximately 1 ms from the data, but expect to see significant modelling error from source/receiver geometry errors and modelling errors.

Solution of the inverse problem employed 128 ensemble members, and required seven iterations to reach the 3 ms noise level. Data and fits are shown in Figs 7(c), (e), (g). Together, these show that as the assumed noise level is lowered, the data are progressively better fit and the model becomes progressively more featured, without developing obvious artefacts related to lack of sufficient regularization. A traditional tomographic reconstruction (again using DWTomo) is shown in Fig. 7(b) and exhibits similar qualitative behaviour to the 3 ms level set/EKI result, with a slow surface layer with similar undulations and a steep step up across the SAF of a faster third layer.

These results show that our parametrization and optimization scheme is sufficiently robust to apply to real inverse problems. At the 3 ms noise level, all significant features of the data are captured even by the relatively simple three layered model proposed here. Lowering the assumed noise level does not significantly qualitatively change the models, but instead sharpens features, especially the primary feature of the step in the fastest velocity across the fault. The initial ensemble of models for all noise levels have on average flat interfaces across the layer boundaries—the progression in Figs 7(d), (f), (h) illustrates a key property of the iteratively EKI algorithm, in that it evolves the ensemble away from the typically smooth ‘prior’ towards a more featured final model. At higher noise levels, this progression is terminated earlier, and so the ensemble will look more like the smooth prior; hence Fig. 7(d) has smoother

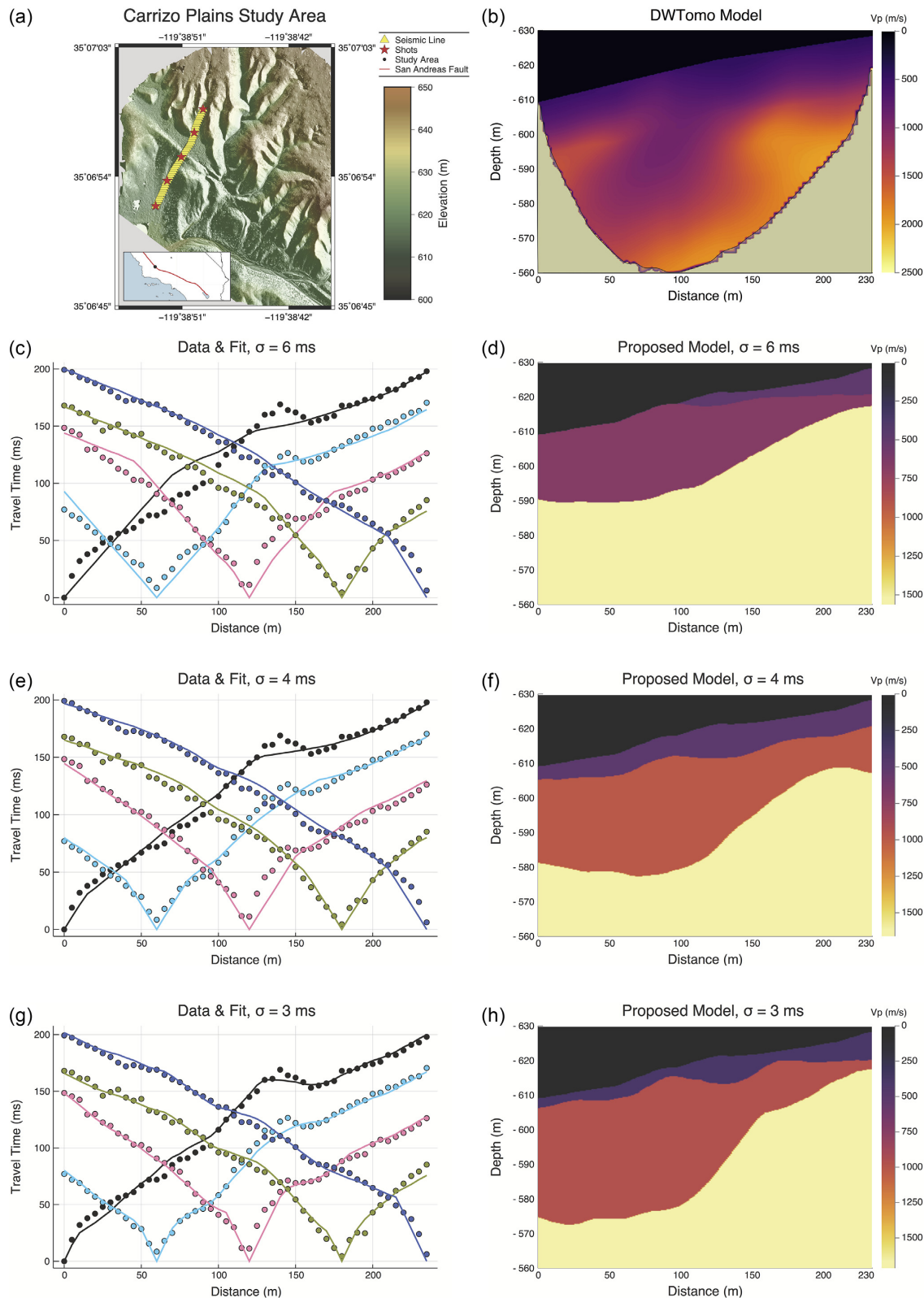


Figure 7. Three layer inversion of near surface velocity adjacent to the San Andreas Fault at Carrizo Plains, illustrating the consistent convergence properties of the iteratively regularized EKI scheme. The black regions of the tomographic images are not inverted, and correspond to air. (a) The study area and source/receiver geometry. (b) The traditional inversion using DWTomato; the opaque grey mask shows the boundary of the rays calculated by DWTomato. (c), (e), and (g) The data and fits for assumed data noise $\sigma = 6, 4, 3$ ms, respectively, and (d), (f), and (h) the corresponding three layer inversion models using our scheme.

and flatter interfaces than Figs 7(f) and (h), in which the evolution of the ensemble progresses further away from the prior. As in any iterative tomographic method, the starting model, or in this case starting ensemble, has an important impact on the final result when the data are noisy, but becomes progressively less important as the inversion is constrained to closely fit the data; a substantial difference to traditional tomographic methods is that the final model produced by EKI lies in the linear span of the starting ensemble, so that for implicit GRF parametrizations the covariance structure is maintained throughout the inversion. This may or may not be a desired property of the inversion; if the initial ensemble encodes a model appropriate for the data then the linear span property ensures that the final model reflects the initial ensemble. Alternatively, if greater flexibility is required due to less strong *a priori* constraints on the model, then a hierarchical generalization of EKI may be employed in which hyperparameters are optimized for the fundamental properties of the parametrization, such as the length scales ρ used for GRFs (Chada *et al.* 2018). As our focus in this study is setting up a general modelling framework, we have chosen not to investigate these generalizations in this paper, however, they offer an intriguing extension for situations in which *a priori* information is relatively lacking.

5 DISCUSSION AND CONCLUSIONS

The objective of this study has been to develop a framework for encoding geological information into geophysical inverse problems in an intuitive way. Using the EKI algorithm, the computational difficulties of taking derivatives of our models are avoided, enabling our definitions to be used to solve large-scale inverse problems defined by nonlinear, possibly black-box forward models. Using our inversion framework we solved three example inverse problems using the *P* wave first arrival traveltime problem as a test case. In these examples, the level-set model specification enabled complex boundaries to be inverted using only the *a priori* knowledge of the expected number of domains. Furthermore, we showed how we can incorporate useful *a priori* information, such as the presence of faults, to deliver a yet more parsimonious model that has significantly better resolution than traditional tomographic approaches. We have illustrated how using our inversion framework appropriately may result in tomographic images that are easier to interpret than traditional images produced by standard methods; the practitioner should be empowered to formulate descriptive models that enable targeted exploration of the data. For conceptual clarity, this study has used examples for which heterogeneity within model regions is sufficiently weak that it is reasonable to assume constant velocity models. However, the model framework permits arbitrary structure within each model layer, which could be modelled with a GRF with no level set function applied. For regions in which there is substantial in-layer heterogeneity, explicit modelling of material interfaces may still be useful when there is a mixture of sharp transitions and smooth variations in mechanical properties which are both relevant to the inverted data—for example, when jointly inverting high-frequency receiver functions with surface wave dispersion for sedimentary basin geometry and internal velocity structure.

One important outcome of the framework not presented in this study is the possibility of formal model selection performed on geologically parameterized models. In the context of model selection, a practitioner would propose several distinct geological models and then use some criterion to rank the models in a preferred order by balancing their complexity against their ability to predict the data. For the deterministic inverse problems solved in this study, which

produce a single optimum model that best fits the model given observed data and prior constraints, various information criterion (IC) such as the Akaike or Bayesian IC may be used (Claeskens 2016). If computational resources permit, cross-validation techniques are possible and act as a guard against outlier data (Claeskens 2016). If a Bayesian approach is taken, more robust approaches include predictive performance checks using draws from the posterior predictive distribution of the data—methods such as PSIS-LOO using these draws can emulate leave-one-out crossvalidation without explicitly resampling the posterior conditioned on subsets of the data (Vehtari *et al.* 2017). Finally, explicit Bayes factor estimation may be tractable for lower dimensionality models where the practitioner is confident in the priors assigned to the model (Weinberg 2012). As our experimental evidence shows, even relatively simple models of the Earth can match complex data to within a realistic noise level. It is therefore up to the domain expertise of the inversion practitioner to design candidate models such that any model selection is meaningful. Once appropriate geophysical models are identified from *a priori* knowledge, our study provides a framework by which the models can be defined and optimized to fit the data. The inversion philosophy promoted by this work is more investigative than exploratory when compared to traditional geophysical inversion procedures that typically emphasize removing *a priori* information as much as possible from the inverse problem. As our understanding of the Earth and its structures grows, we believe that methodologies, such as the one presented here, that are driven by our *a priori* knowledge will become increasingly important to ameliorate the fundamental issue of non-uniqueness in geophysical inverse problems.

ACKNOWLEDGEMENTS AND FUNDING SOURCES

The authors would like to thank Nicholas Rawlinson and an anonymous reviewer for providing useful commentary that has significantly improved the quality of the manuscript. We would also like to thank Editor Michael Ritzwoller and the anonymous assistant editor for managing the review process. JBM would like to thank Andrew Stuart (Caltech Computational and Mathematical Sciences) and the 2018 Gene Golub SIAM summer school for useful discussions regarding this study. Data from Carrizo Plains was collected during the 2017 Caltech Applied Geophysics Field Course, for which JBM was a Teaching Assistant. JBM would like to thank the instructors Rob Clayton and Mark Simons, and co-TA Voon Hui Lai, as well as the students, for the course. JBM would also like to thank the General Sir John Monash Foundation and the Origin Energy Foundation for financial support. This study was supported by NSF grant EAR-1453263.

RESOURCES

All calculations were computed using the Julia language (Bezanson *et al.* 2017). Code for our model specification language can be found at <https://github.com/jbmuir/EarthModels.jl>. Code for the EKI optimizer can be found at <https://github.com/jbmuir/EnsembleKalmanInversion.jl>. Code for a Julia 1.0+ compliant factored Eikonal fast marching method forward solver can be found at <https://github.com/jbmuir/FEFMM.jl>.

REFERENCES

Akciz, S.O., Grant Ludwig, L. & Arrowsmith, J.R., 2009. Revised dates of large earthquakes along the Carrizo section of the San Andreas

- Fault, California, since A.D. 1310 \pm 30, *J. geophys. Res.*, **114**(B1), doi:10.1029/2007JB005285.
- Aki, K., Christofferson, A. & Husebye, E.S., 1977. Determination of the three-dimensional seismic structure of the lithosphere, *J. geophys. Res.*, **82**(2), 277–296.
- Backus, G. & Gilbert, F., 1968. The resolving power of gross earth data, *J. geophys. Int.*, **16**(2), 169–205.
- Bezanson, J., Edelman, A., Karpinski, S. & Shah, V.B., 2017. Julia: a fresh approach to numerical computing, *SIAM Rev.*, **59**(1), 65–98.
- Bianco, M.J. & Gerstoft, P., 2018. Travel time tomography with adaptive dictionaries, *IEEE Trans. Comput. Imaging*, **4**(4), 499–511.
- Bodin, T. & Sambridge, M., 2009. Seismic tomography with the reversible jump algorithm, *J. geophys. Int.*, **178**(3), 1411–1436.
- Cardiff, M. & Kitanidis, P.K., 2009. Bayesian inversion for facies detection: an extensible level set framework, *Water Resour. Res.*, **45**(10), doi:10.1029/2008WR007675.
- Chada, N.K., Iglesias, M.A., Roininen, L. & Stuart, A.M., 2018. Parameterizations for ensemble Kalman inversion, *Inverse Probl.*, **34**(5), 055009, doi:10.1088/1361-6420/aa6d9.
- Chiles, J.-P. & Delfiner, P., 2012. *Geostatistics: Modeling Spatial Uncertainty*, Vol. 497, 2nd edn, John Wiley & Sons.
- Chung, E.T., Chan, T.F. & Tai, X.-C., 2005. Electrical impedance tomography using level set representation and total variational regularization, *J. Comput. Phys.*, **205**(1), 357–372.
- Claeskens, G., 2016. Statistical model choice, *Annu. Rev. Stat. Appl.*, **3**(1), 233–256.
- de Wit, R.W.L., Trampert, J. & van der Hilst, R.D., 2012. Toward quantifying uncertainty in travel time tomography using the null-space shuttle: Robustness in travel time tomography, *J. geophys. Res.*, **117**(B3), doi:10.1029/2011JB008754.
- Deal, M.M. & Nolet, G., 1996. Nullspace shuttles, *J. geophys. Int.*, **124**(2), 372–380.
- Dziewonski, A.M., Hager, B.H. & O’Connell, R.J., 1977. Large-scale heterogeneities in the lower mantle, *J. geophys. Res.*, **82**(2), 239–255.
- Eikrem, K.S., Nævdal, G. & Jakobsen, M., 2019. Iterated extended Kalman filter method for time-lapse seismic full waveform inversion, *Geophys. Prospect.*, **67**, 379–394.
- Evensen, G., 1994. Sequential data assimilation with a nonlinear quasi-geostrophic model using Monte Carlo methods to forecast error statistics, *J. geophys. Res.*, **99**(C5), 10143–10162.
- Fichtner, A. & Zunino, A., 2019. Hamiltonian nullspace shuttles, *Geophys. Res. Lett.*, **46**(2), 644–651.
- Foulger, G.R. et al., 2013. Caveats on tomographic images, *Terra Nova*, **25**(4), 259–281.
- Gao, C. & Lekić, V., 2018. Consequences of parameterization choices in surface wave inversion: Insights from transdimensional Bayesian methods, *J. geophys. Int.*, **215**(2), 1037–1063.
- Geogiga Technology Corporation, 2016. *DWTomo*. Available at: <http://geogiga.com/en/dwtomo.php> (last accessed 2019 November 11).
- Halko, N., Martinsson, P.G. & Tropp, J.A., 2011. Finding structure with randomness: probabilistic algorithms for constructing approximate matrix decompositions, *SIAM Rev.*, **53**(2), 217–288.
- Hanke, M., 1997. A regularizing Levenberg–Marquardt scheme, with applications to inverse groundwater filtration problems, *Inverse Probl.*, **13**(1), 79–95.
- Hansen, T.M., Journel, A.G., Tarantola, A. & Mosegaard, K., 2006. Linear inverse Gaussian theory and geostatistics, *Geophysics*, **71**(6), R101–R111.
- Herlihy, M. & Shavit, N., 2011. *The Art of Multiprocessor Programming*, Morgan Kaufmann.
- Iglesias, M.A., 2015. Iterative regularization for ensemble data assimilation in reservoir models, *Comput. Geosci.*, **19**(1), 177–212.
- Iglesias, M.A., 2016. A regularizing iterative ensemble Kalman method for PDE-constrained inverse problems, *Inverse Probl.*, **32**(2), 025002, doi:10.1088/0266-5611/32/2/025002.
- Iglesias, M.A. & Dawson, C., 2013. The regularizing Levenberg–Marquardt scheme for history matching of petroleum reservoirs, *Comput. Geosci.*, **17**(6), 1033–1053.
- Iglesias, M.A., Law, K.J.H. & Stuart, A.M., 2013. Ensemble Kalman methods for inverse problems, *Inverse Probl.*, **29**(4), 045001, doi:10.1088/0266-5611/29/4/045001.
- Isakov, V., Leung, S. & Qian, J., 2011. A fast local level set method for inverse gravimetry, *Commun. Comput. Phys.*, **10**(04), 1044–1070.
- Ko, J.Y.-T., Helmberger, D.V., Wang, H. & Zhan, Z., 2017. Lower mantle substructure embedded in the farallon plate: the Hess conjugate, *Geophys. Res. Lett.*, **44**(20), 10216–10225.
- Komatitsch, D., Xie, Z., Bozdağ, E., Sales de Andrade, E., Peter, D., Liu, Q. & Tromp, J., 2016. Anelastic sensitivity kernels with parsimonious storage for adjoint tomography and full waveform inversion, *J. geophys. Int.*, **206**(3), 1467–1478.
- Kovachki, N.B. & Stuart, A.M., 2019. Ensemble Kalman inversion: a derivative-free technique for machine learning tasks, *Inverse Probl.*, **35**, doi:10.1088/1361-6420/ab1c3a.
- Li, W. & Qian, J., 2016. Joint inversion of gravity and traveltime data using a level-set-based structural parameterization, *Geophysics*, **81**(6), G107–G119.
- Li, W., Leung, S. & Qian, J., 2014. A level-set adjoint-state method for crosswell transmission-reflection traveltime tomography, *J. geophys. Int.*, **199**(1), 348–367.
- Li, W., Lu, W., Qian, J. & Li, Y., 2017. A multiple level-set method for 3D inversion of magnetic data, *Geophysics*, **82**(5), J61–J81.
- Lu, W. & Qian, J., 2015. A local level-set method for 3D inversion of gravity-gradient data, *Geophysics*, **80**(1), G35–G51.
- Ludwig, L.G., Akciz, S.O., Noriega, G.R., Zielke, O. & Arrowsmith, J.R., 2010. Climate-Modulated Channel Incision and Rupture History of the San Andreas Fault in the Carrizo Plain, *Science*, **327**(5969), 1117–1119.
- Ni, S., Tan, E., Gurnis, M. & Helmberger, D., 2002. Sharp Sides to the African Superplume, *Science*, **296**(5574), 1850–1852.
- Osher, S. & Sethian, J.A., 1988. Fronts propagating with curvature-dependent speed: Algorithms based on Hamilton–Jacobi formulations, *J. Comput. Phys.*, **79**(1), 12–49.
- Osher, S., Burger, M., Goldfarb, D., Xu, J. & Yin, W., 2005. An iterative regularization method for total variation-based image restoration, *Multiscale Model. Simul.*, **4**(2), 460–489.
- Parker, R.L., 1994. *Geophysical Inverse Theory*, Princeton Univ. Press.
- Rasmussen, C.E. & Williams, C.K.I., 2006. *Gaussian Processes for Machine Learning, Adaptive Computation and Machine Learning*, MIT Press.
- Rawlinson, N. & Sambridge, M., 2004. Wave front evolution in strongly heterogeneous layered media using the fast marching method, *J. geophys. Int.*, **156**(3), 631–647.
- Rawlinson, N., Pozgay, S. & Fishwick, S., 2010. Seismic tomography: A window into deep Earth, *Phys. Earth Planet. Inter.*, **178**(3–4), 101–135.
- Rawlinson, N., Fichtner, A., Sambridge, M. & Young, M.K., 2014. Seismic tomography and the assessment of uncertainty, *Adv. Geophys.*, **55**, 1–76.
- Ray, A. & Myer, D., 2019. Bayesian geophysical inversion with transdimensional Gaussian Process machine learning, *J. geophys. Int.*, **217**(3), 1706–1725.
- Roy, C. & Romanowicz, B.A., 2017. On the implications of *a priori* constraints in transdimensional Bayesian inversion for continental lithospheric layering, *J. geophys. Res.*, **122**(12), 10118–10131.
- Scherzer, O., 1993. The use of Morozov’s discrepancy principle for Tikhonov regularization for solving nonlinear ill-posed problems, *Computing*, **51**(1), 45–60.
- Song, T.-R.A., Helmberger, D.V., Brudzinski, M.R., Clayton, R.W., Davis, P., Perez-Campos, X. & Singh, S.K., 2009. Subducting slab ultra-slow velocity layer coincident with silent earthquakes in Southern Mexico, *Science*, **324**(5926), 502–506.
- Sun, D., Helmberger, D., Miller, M.S. & Jackson, J.M., 2016. Major disruption of D'' beneath Alaska, *J. geophys. Res.*, **121**(5), 3534–3556.
- Tarantola, A., 2005. *Inverse Problem Theory and Methods for Model Parameter Estimation*, SIAM.
- Thurin, J., Brossier, R. & Métivier, L., 2017. An ensemble-transform Kalman filter: Full-waveform inversion scheme for uncertainty estimation, in *SEG Technical Program Expanded Abstracts 2017*, Society of Exploration Geophysicists, Houston, Texas, pp. 1307–1313.

- Treister, E. & Haber, E., 2016. A fast marching algorithm for the factored eikonal equation, *J. Comput. Phys.*, **324**, 210–225.
- Vehtari, A., Gelman, A. & Gabry, J., 2017. Practical Bayesian model evaluation using leave-one-out cross-validation and WAIC, *Stat. Comput.*, **27**(5), 1413–1432.
- Weinberg, M.D., 2012. Computing the Bayes Factor from a Markov Chain Monte Carlo Simulation of the Posterior Distribution, *Bayesian Anal.*, **7**(3), 737–770.
- Zelt, C.A. & Smith, R.B., 1992. Seismic traveltime inversion for 2-D crustal velocity structure, *J. geophys. Int.*, **108**(1), 16–34.
- Zheglova, P., Farquharson, C.G. & Hurich, C.A., 2013. 2-D reconstruction of boundaries with level set inversion of traveltimes, *J. geophys. Int.*, **192**(2), 688–698.
- Zheglova, P., Lelièvre, P.G. & Farquharson, C.G., 2018. Multiple level-set joint inversion of traveltime and gravity data with application to ore delineation: A synthetic study, *Geophysics*, **83**(1), R13–R30.
- Zielke, O., Arrowsmith, J.R., Ludwig, L.G. & Akciz, S.O., 2010. Slip in the 1857 and Earlier Large Earthquakes Along the Carrizo Plain, San Andreas Fault, *Science*, **327**(5969), 1119–1122.

APPENDIX

A1 Combinatorial definition of multiple level sets

For N regional parameter fields of interest, set n such that $N = 2^n$. If N is not a power of 2, we can arbitrarily split regions until we can meet this condition; this will generate a ‘boundary’ without a discontinuity across it. We define the Heaviside step operator to be

$$H(\phi)(x) = \begin{cases} 1, & \phi(x) > 0 \\ 0, & \phi(x) \leq 0 \end{cases}. \quad (\text{A1})$$

Then let $\iota(i, j)$ be the i th digit of the binary representation of $j - 1$. Then

$$F(x) = \sum_{j=1}^N \prod_{i=1}^n A_j(x) \iota(i, j) (1 - H(\phi_i)(x)) + (1 - \iota(i, j)) H(\phi_i)(x). \quad (\text{A2})$$

This definition is differentiable and potentially requires fewer auxiliary fields than the procedural definition. However, due to the combinatoric nature of the formula differentiation becomes difficult in practice for $n > 2$, and regularization of the inverse problem may result in cross-talk between different regions which share some

of the same auxiliary fields—auxiliary fields are not individually associated with regional parameter fields.

A2 Derivation of explicit Levenberg–Marquardt update in finite dimensions

In finite dimensions, Γ and C are symmetric positive-definite matrices. For compactness, let the prediction error at u_n be $y - G(u_n) = \delta y_n$. We start with the LM update rule in finite dimensions

$$u_{n+1} = u + v^*, \quad (\text{A3})$$

$$v^* = \arg \min_{v \in \mathbb{R}^M} (\|\Gamma^{-1/2}(\delta y_n - J(u_n)v)\|_{\mathbb{R}^M}^2 + \alpha_n \|C^{-1/2}v\|_{\mathbb{R}^N}^2), \quad (\text{A4})$$

$$v^* = \arg \min_{v \in \mathbb{R}^M} ((\delta y_n - J(u_n)v)^T \Gamma^{-1} (\delta y_n - J(u_n)v) + \alpha_n v^T C^{-1} v). \quad (\text{A5})$$

The condition for v^* is that the derivative of the right-hand side equals 0, which gives

$$\frac{\partial ((\delta y_n - J(u_n)v)^T \Gamma^{-1} (\delta y_n - J(u_n)v) + \alpha_n v^T C^{-1} v)}{\partial v} \quad (\text{A6})$$

$$= \frac{\partial (\delta y_n - J(u_n)v)^T \Gamma^{-1} (\delta y_n - J(u_n)v)}{\partial (\delta y_n - J(u_n)v)} \frac{\partial (\delta y_n - J(u_n)v)}{\partial v} + \frac{\partial \alpha_n v^T C^{-1} v}{\partial v} \quad (\text{A7})$$

$$= -(\delta y_n - J(u_n)v)^T \Gamma^{-1} J(u_n) + \alpha_n v^T C^{-1} \quad (\text{A8})$$

$$= v^T (J(u_n)^T \Gamma^{-1} J(u_n) + \alpha_n C^{-1}) - \delta y_n^T \Gamma^{-1} J(u_n) \quad (\text{A9})$$

$$= 0, \quad (\text{A10})$$

or on taking transposes while noting Γ^{-1} and C^{-1} are both symmetric

$$(J(u_n)^T \Gamma^{-1} J(u_n) + \alpha_n C^{-1})v = J(u_n)^T \Gamma^{-1} \delta y_n, \quad (\text{A11})$$

which gives the usual explicit LM update

$$v^* = (J(u_n)^T \Gamma^{-1} J(u_n) + \alpha_n C^{-1})^{-1} J(u_n)^T \Gamma^{-1} (y - G(u_n)). \quad (\text{A12})$$